Supplementary figures

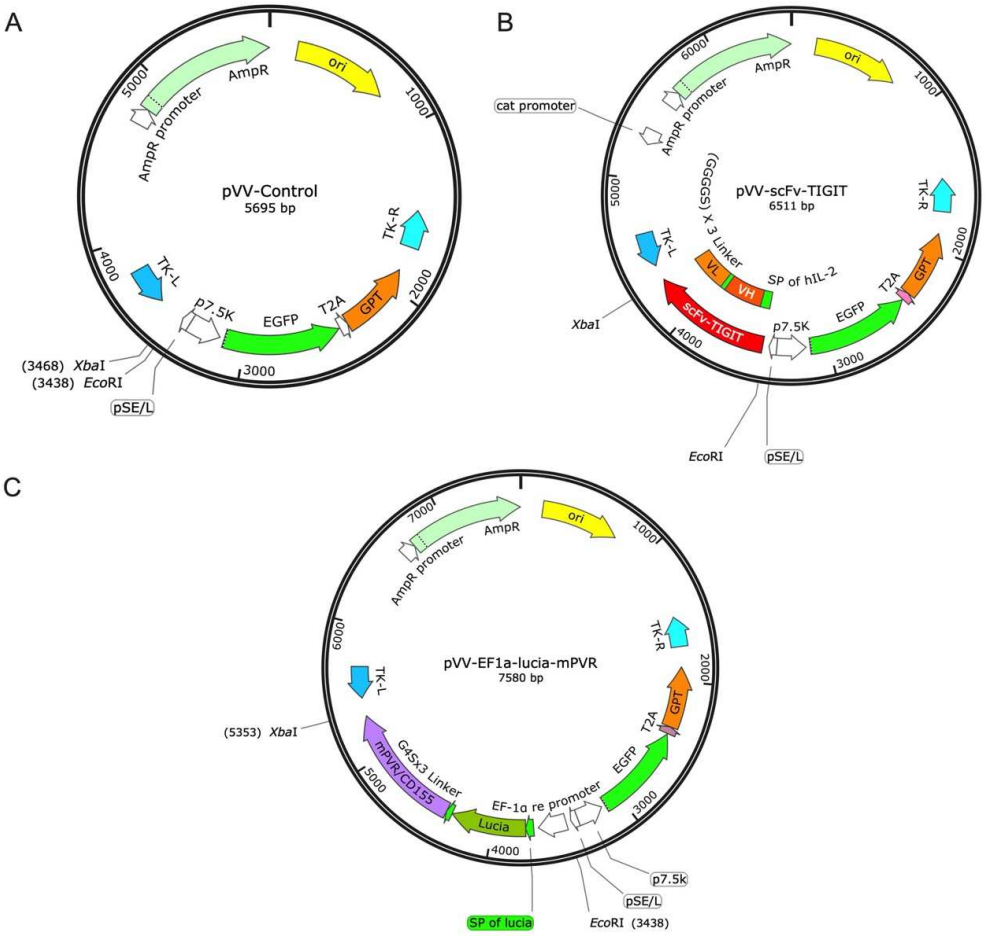

Fig. S1 Map of shuttle plasmids for construction of the recombinant vaccinia virus or expression of mPVR/CD155. (A) Map of pVV-Control. (B) Map of pVV-scFv-TIGIT. (C) Map of pVV-EF1a-lucia-mPVR.

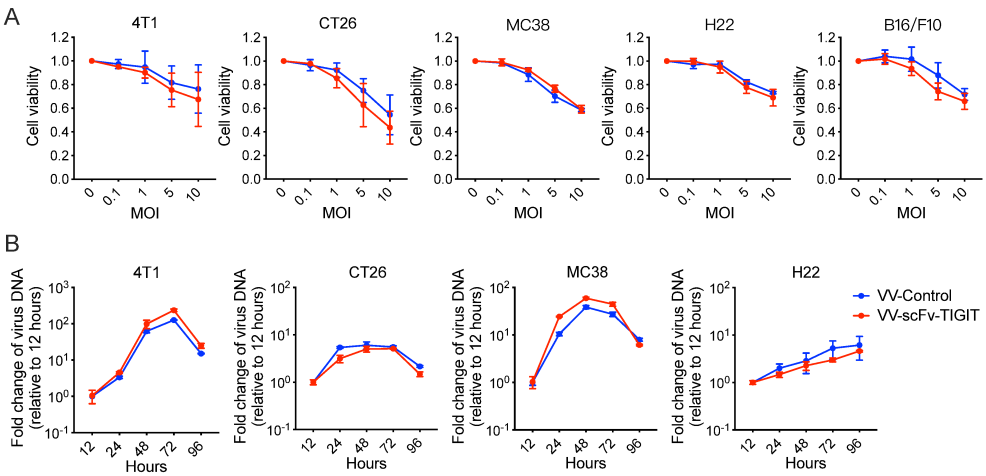

Fig. S2 The replication and oncolytic ability of VVs in mouse tumor cells. (A) MTT (for 4T1, CT26, MC38, and B16/F10 cells) and CCK8 assays (for H22 cells) were used to detect the oncolytic ability of VVs against mouse tumor cells. (B) qPCR was used to detect viral replication in murine tumor cells.

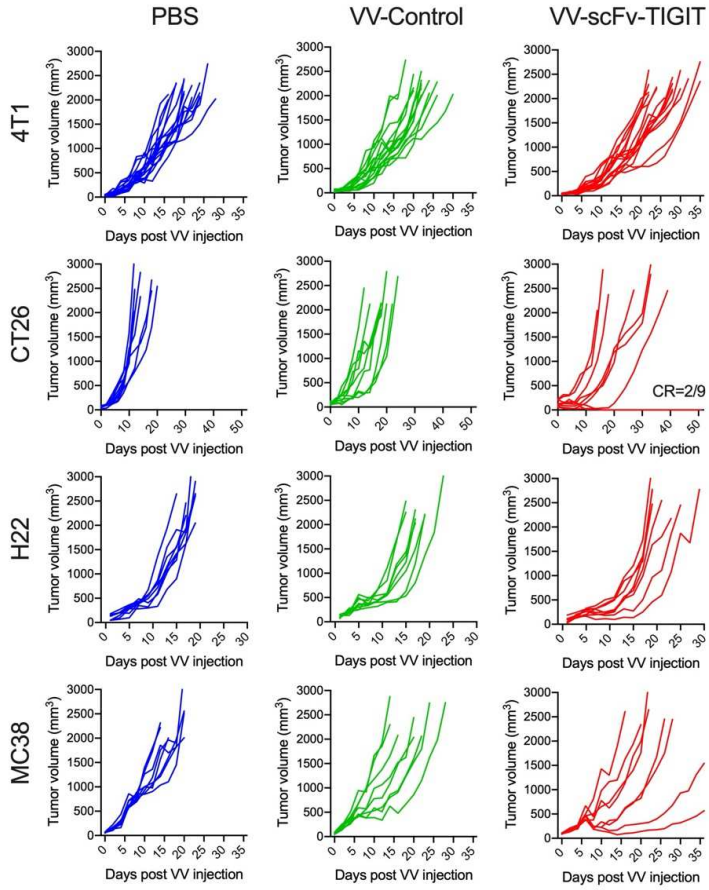

Fig. S3 Individual tumor growth curve of mice. The establishment of the tumor model and the treatment scheme were similar to Fig. 2A. The tumor volume was measured every two days. Once the tumor volume of the mouse exceeded 2000 mm^3, it was no longer measured. CR, complete remission.

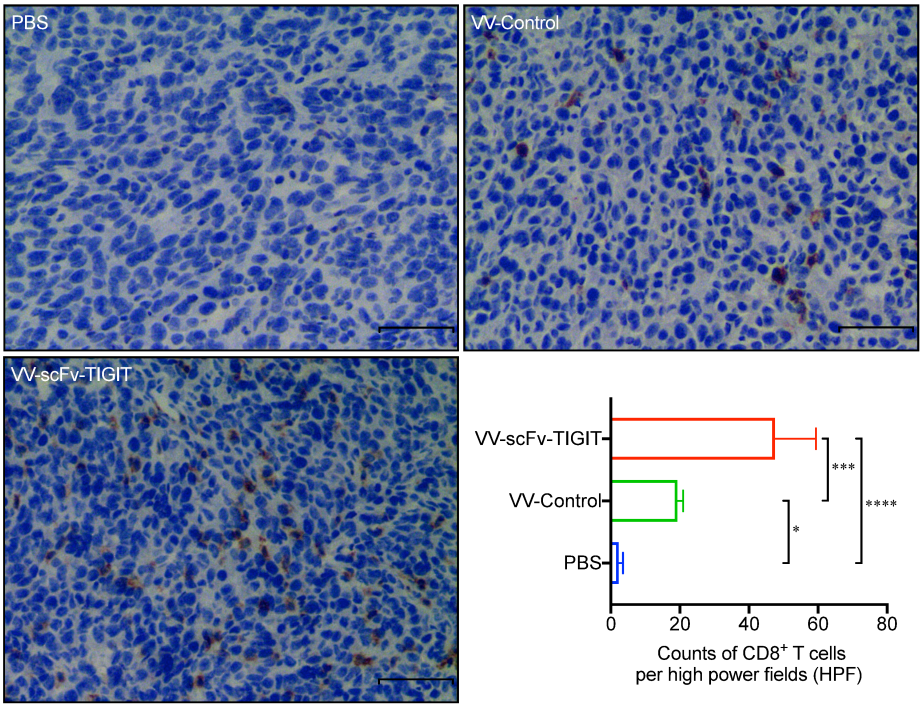

Fig. S4. Measurement of the infiltration of CD8⁺ T cells. The establishment of the tumor model (CT26) and the treatment scheme was similar to Fig. 3A. Immunohistochemical (IHC) staining was used to detect the infiltration of CD8⁺ T cells in the tumor tissue of the CT26 subcutaneous model. Representative image of high magnification (400×). Scale bar represents 50 μm. $^{*}P < 0.05$; $^{***}P < 0.001$; $^{****}P < 0.0001$.

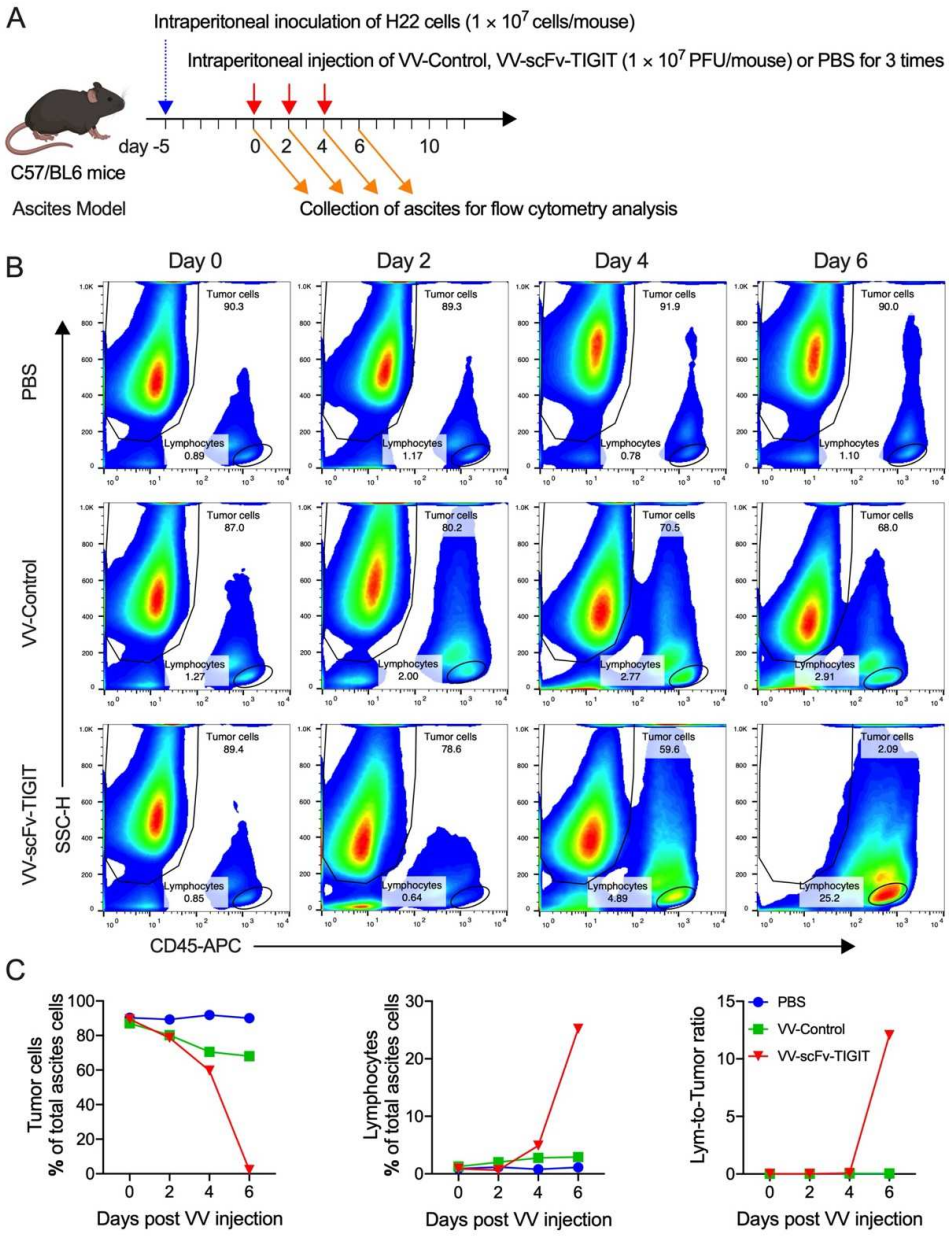

Fig. S5 Dynamic analysis of the proportion of tumor cells and lymphocytes in ascites. (A) Treatment scheme of H22 ascites model. (B) Representative diagram of flow cytometric analysis of tumor cells and lymphocytes in the ascites. (C) The dynamic curve of tumor cells, lymphocytes, and the lymphocyte-to-tumor ratio.

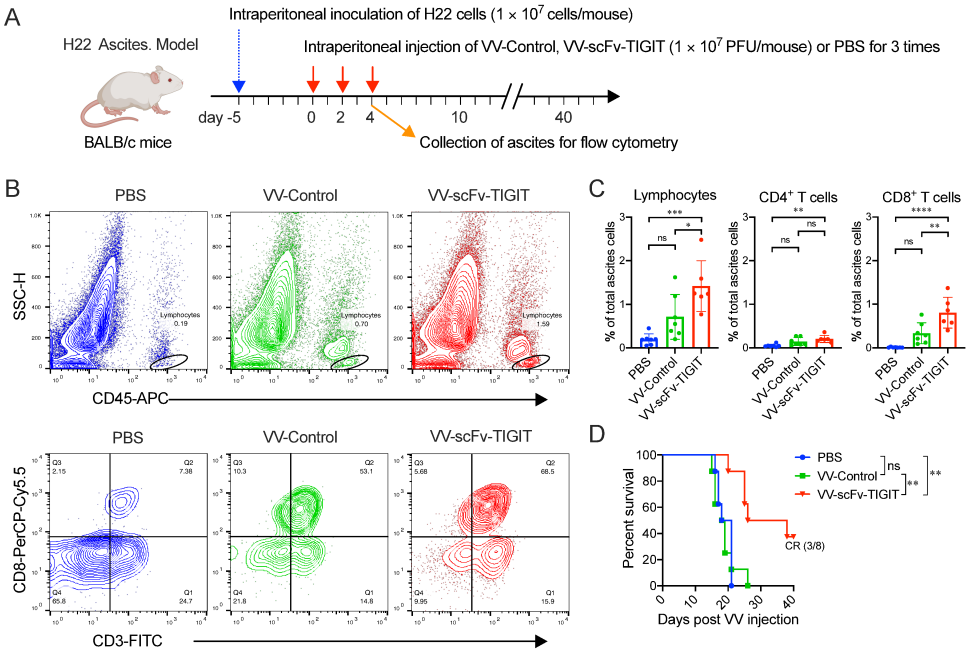

Fig. S6 Enhanced anti-tumor efficacy of VV-scFv-TIGIT on ascites tumor model in BALB/c mice (A) Treatment scheme. (B) Representative diagram of flow cytometric analysis of lymphocytes and their subsets in the ascites at day 4 post the first VV injection (before the third VV injection). (C) Flow cytometric analysis of the proportion of lymphocytes and their subsets in the ascites. (D) Kaplan-Meier survival curves of tumor-bearing mice. ns, no significant differences; $^{*}P < 0.05$; $^{**}P < 0.01$; $^{***}P < 0.001$; $^{****}P < 0.0001$.

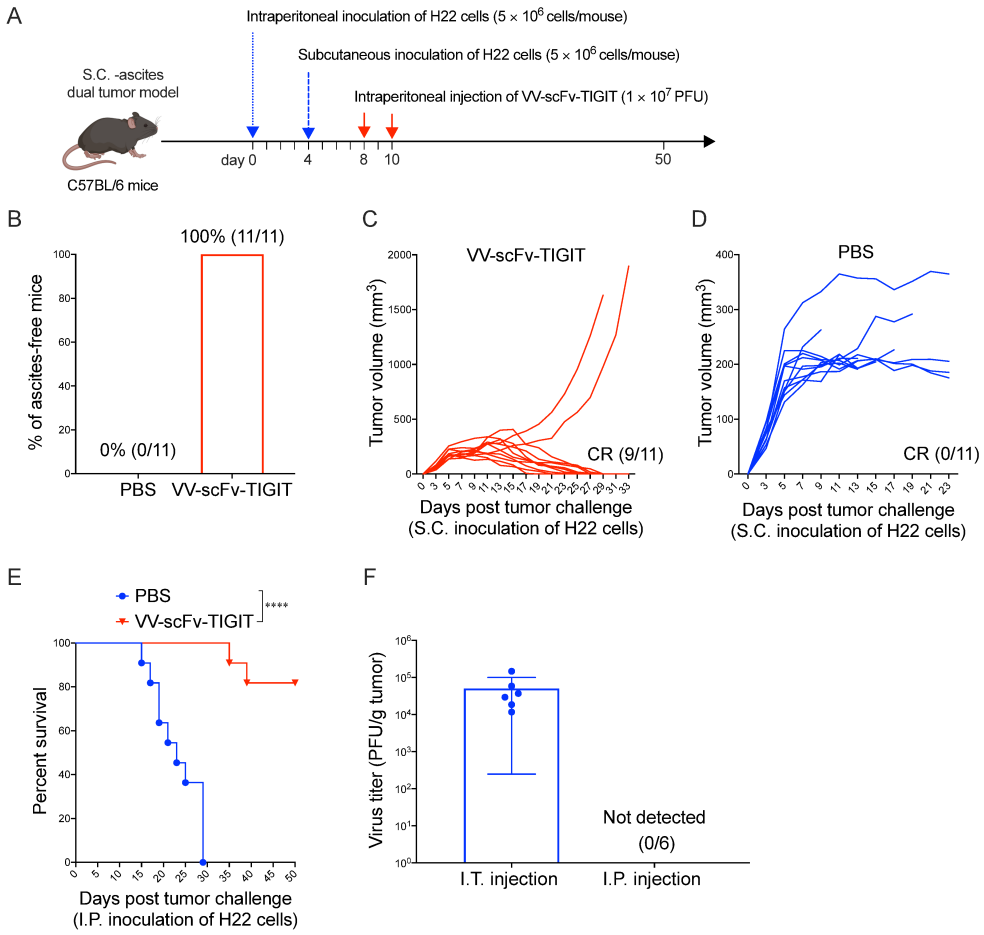

Fig. S7 Efficacy of VV-scFv-TIGIT on subcutaneous-ascites dual tumor model. (A) Treatment scheme of the subcutaneous-ascites dual tumor model. (B) Percentage of ascites-free mice after treatment with VV-scFv-TIGIT or PBS. (C, D) Tumor growth curve of individual mice. (E) Kaplan-Meier survival curves of mice. $^{****}P < 0.0001$. (F) Virus titers in the subcutaneous tumor. The subcutaneous-ascites dual tumor model was established as (A). Four days post subcutaneous inoculation of H22 cells, 1×10^7 PFU of VV-scFv-TIGIT was intraperitoneally (I.P.) injected into mice or intratumorally (I.T.) injected into the subcutaneous tumor. Three days post virus injection, mice (6 for each group) were sacrificed and the subcutaneous tumor was collected. Then, 100 mg of tumor sample was added with 200 ml PBS and lysed with a homogenizer. After that, the supernatants were separated by centrifugation (3000 × g) and the virus titer was tested using a TCID50 method.

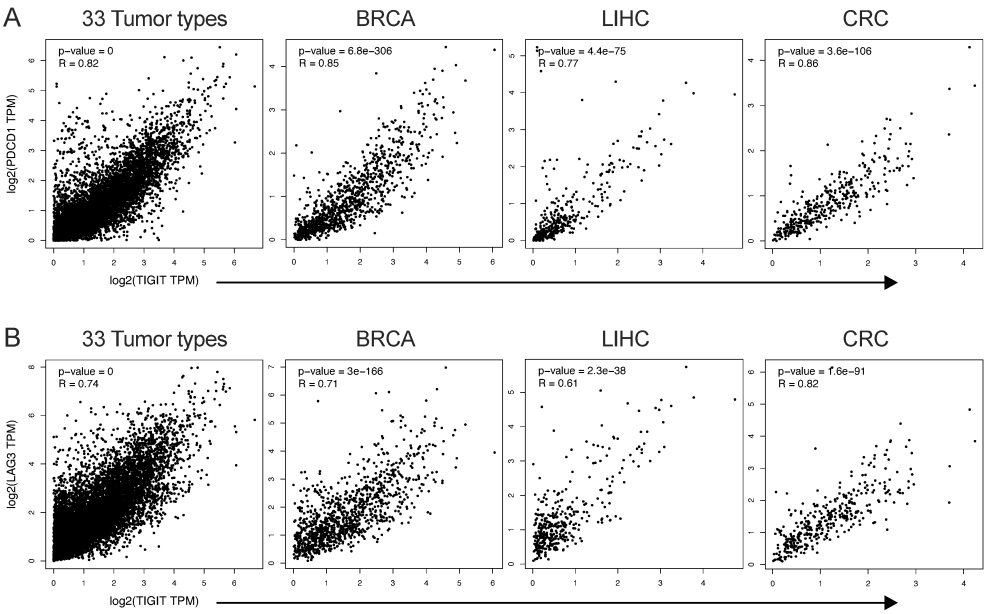

Fig. S8 The correlation of gene expression between immune checkpoints. (A) The correlation of gene expression between TIGIT and PD-1 (PDCD1). (B) The correlation of gene expression between TIGIT and LAG-3. The value of transcription per million (TPM) of gene expression is derived from the RNA-sequencing (RNA-seq) data of tumor tissue in the Cancer Genome Atlas (TCGA). Correlation analysis was performed via GEPIA2 (http://gepia2.cancer-pku.cn) using Spearman's method. R, correlation coefficient; BRCA, breast cancer; CRC, colorectal carcinoma; LIHC, liver hepatocellular carcinoma.

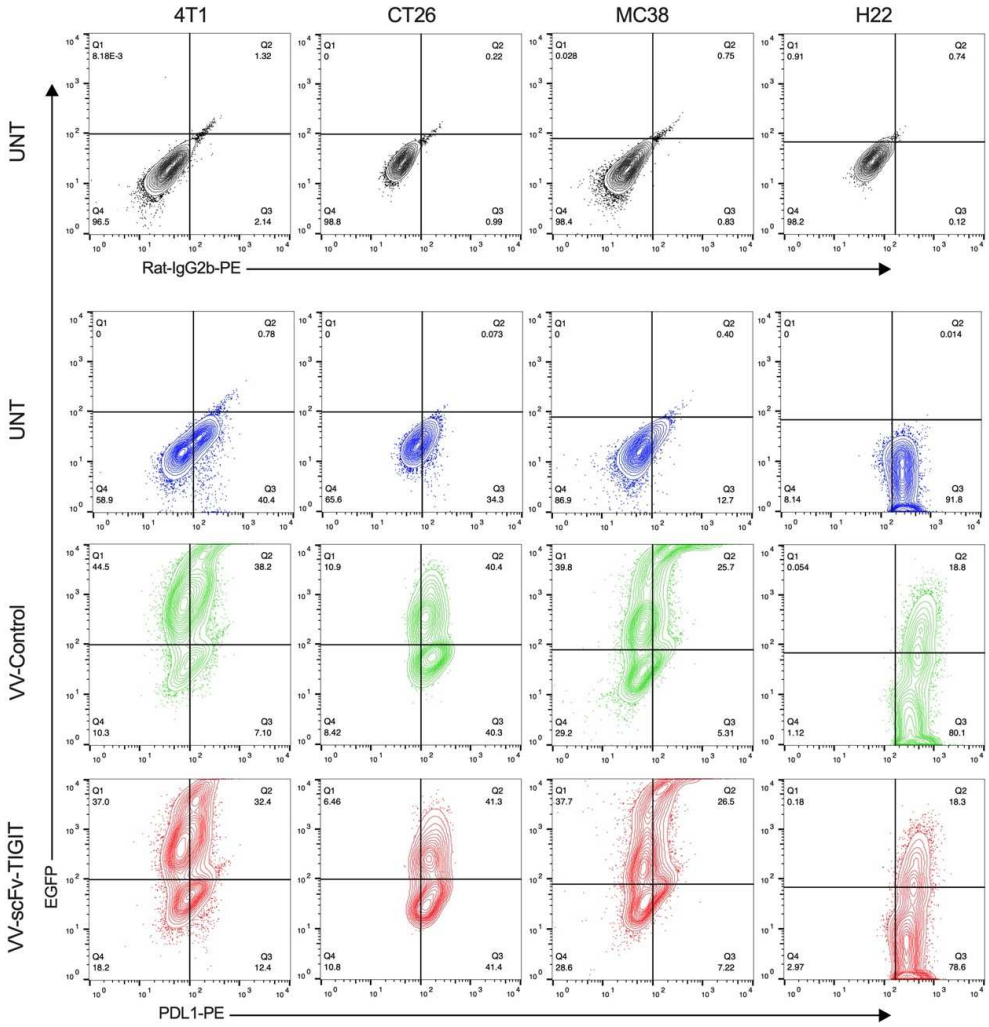

Fig. S9 Up-regulation of PD-L1 expression on tumor cells after VV infection. CT26, MC38, 4T1, and H22 cells were seeded in 6-well plates and infected with indicated VV at a multiplicity of infection (MOI) of 1. After a 48-h incubation, tumor cells were harvested and the expression of PD-L1 on these cells was detected by flow cytometry using a PE-conjugated anti-PD-L1 antibody. PE-conjugated Rat IgG2b was used as an isotype control. UNT, untreated cells.

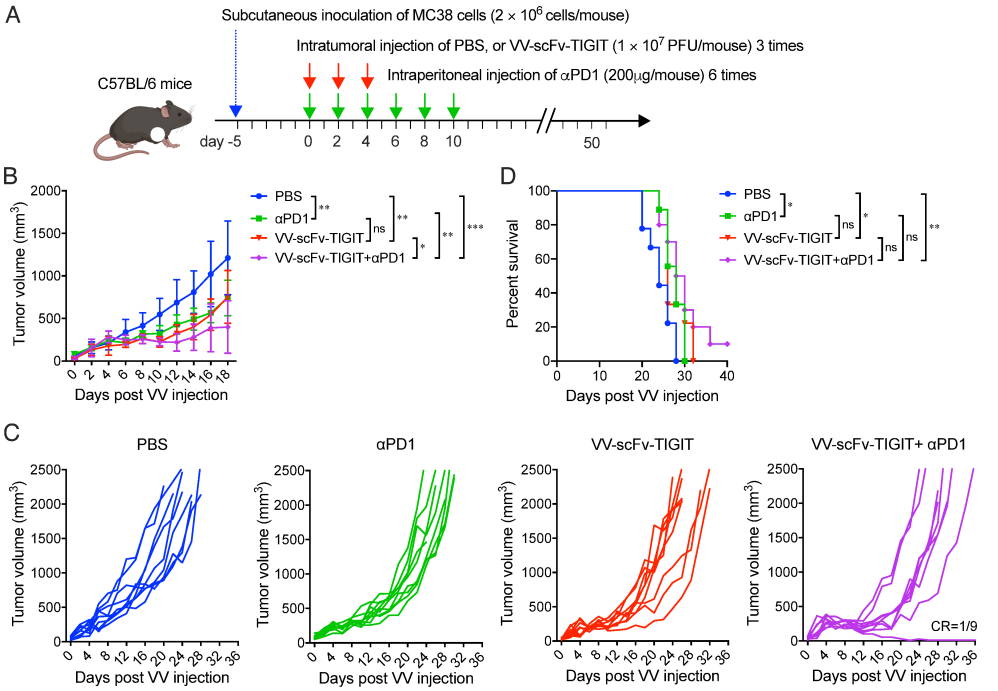

Fig. S10 Combination therapy with αPD-1 improved the anti-tumor efficacy of VV-scFv-TIGIT in the MC38 colon cancer model. (A) Treatment scheme. (B) Mean tumor volume of mice. Tumor volume was measured every two days. Error bars represent standard deviation. (C) Individual tumor growth curve of mice. CR, complete remission. (D) Kaplan-Meier survival curves of tumor-bearing mice. Once the tumor volume exceeded 2000 mm^3, the mouse was considered dead; ns, no significant differences; $^{*}P < 0.05$; $^{**}P < 0.01$.

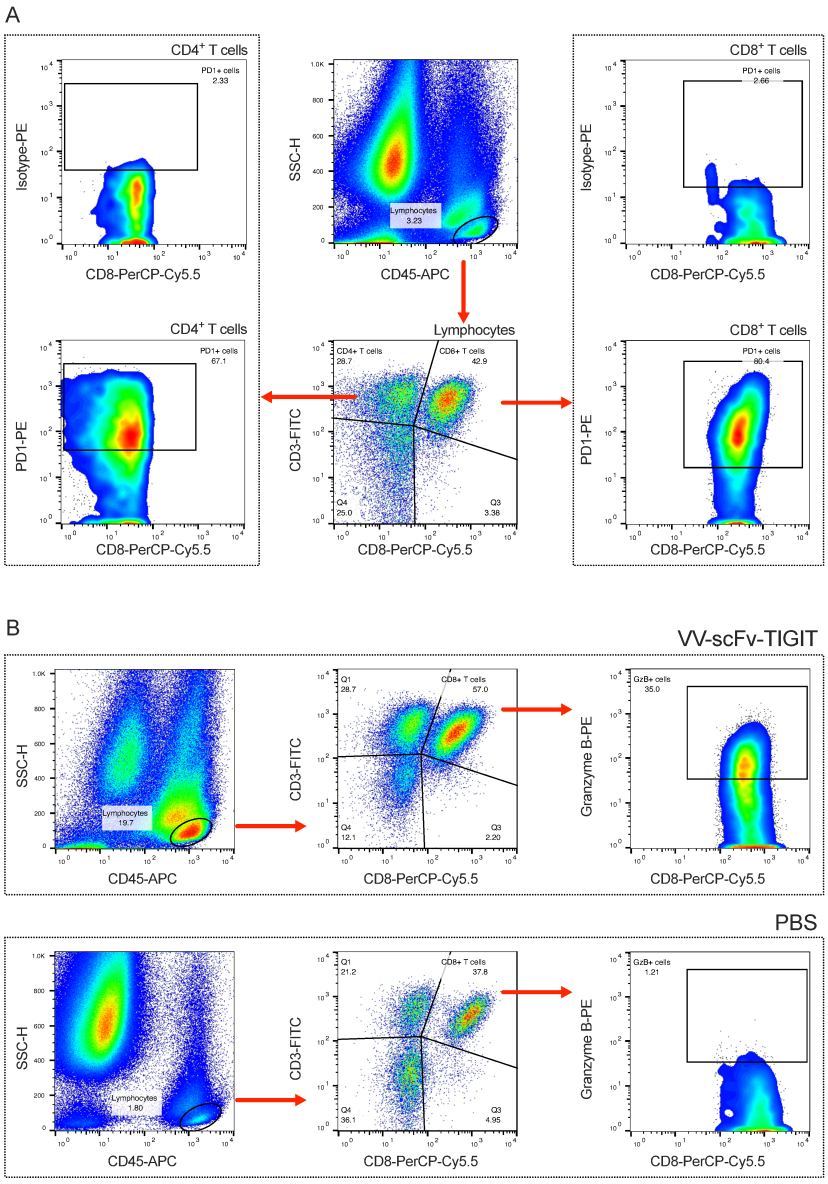

Fig. S11 Representative gating strategy for flow cytometry. (A) Representative gating strategy used to identify the expression of PD1, TIGIT, TIM3, LAG3, and CD107A on $CD4^+$ or $CD8^+$ T cells. (B) Representative gating strategy for intracellular staining of Granzyme B, IFN-γ, and TNF-α in $CD8^+$ T cells.